



ISSN 0077-880X

THE UNIVERSITY OF
NEW SOUTH WALES

STUDIES FROM
SCHOOL OF CIVIL AND ENVIRONMENTAL ENGINEERING

**INELASTIC BUCKLING OF RECTANGULAR STEEL
PLATES USING A RAYLEIGH-RITZ METHOD**

S T SMITH, M A BRADFORD, D J OEHLERS

UNICIV REPORT No. R-387 DECEMBER 1999
THE UNIVERSITY OF NEW SOUTH WALES
SYDNEY 2052 AUSTRALIA

ISBN : 85841 354 X

INELASTIC BUCKLING OF RECTANGULAR STEEL PLATES USING A RAYLEIGH-RITZ METHOD

by

S.T. Smith, BE PhD

*Postdoctoral Research Fellow, Department of Civil and Structural Engineering,
The Hong Kong Polytechnic University, Hong Kong*

M.A. Bradford, BSc BE PhD DSc

Professor of Civil Engineering, UNSW

D.J. Oehlers, MSc PhD

*Senior Lecturer in Civil Engineering, The University of Adelaide, Adelaide, SA
5005*

ABSTRACT

The paper presents a Rayleigh-Ritz based non-discretisation method of analysis for the inelastic local buckling of rectangular steel plates subjected to applied in-plane axial, bending and shear actions with various boundary conditions. Use is made of the pb-2 representation of the displacement function as the product of a domain polynomial and a boundary polynomial. The constitutive model for the plate is an adaptation of the von Mises yield criterion and the associated flow rule presented in an infinitesimal form, and which leads to an incremental and iterative method of solution. The convergence and accuracy of the solutions are demonstrated, and it is shown that the method of analysis is computationally feasible for the solution of inelastic bifurcative plate instability problems. A parametric study is then undertaken for a range of plate boundary conditions under various regimes of applied loading.

KEY WORDS

Buckling, flow theory, inelasticity, plates, Rayleigh-Ritz method, steel.

CONTENTS

1.	Introduction	3
2.	Theory	5
	2.1 General	5
	2.2 Displacement function	5
	2.3 Total change in potential	6
	2.4 Variational solution	7
	2.5 Modelling inelasticity	8
3.	Verification and Convergence	11
	3.1 General	11
	3.2 Elastic buckling	11
	3.3 Convergence	12
4.	Illustration	14
	4.1 General	14
	4.2 Interaction of bending and compression	15
	4.3 Interaction of bending and shear	14
	4.4 Interaction of compression and shear	15
5.	Conclusions	16
6.	Acknowledgements	16
7.	References	17
	APPENDIX 1 – Boundary Polynomial φ_b	20
	APPENDIX 2 – Flexural Stiffness Matrix k_{ij}	21
	Tables	22
	Figures	26

1. Introduction

This paper is concerned with the inelastic local buckling of mild steel plates using a Rayleigh-Ritz procedure that does not require topological discretisation. A polynomial-based displacement function for the elastic (unilateral) buckling of plates against a rigid restraining medium has been used previously by the authors [1], and shown to lead to a well-behaved solution technique for this class of contact problems [2]. The two-dimensional Ritz function is the basis of the pb-2 Rayleigh-Ritz method, which was developed initially by Liew and his colleagues [3,4], and which forms the basis for an efficient technique for the solution of buckling and vibration eigenproblems. The pb-2 Rayleigh-Ritz method is extended in this paper to present a solution technique for the inelastic local buckling of rectangular steel plates.

Traditionally, problems of inelasticity in plate buckling have used either the flow or deformation theories of plasticity [5]. The flow theory of plasticity relates the increments of plastic strain to the stress, and was developed in early work by Handelman and Prager [6]. The deformation theory of plasticity, on the other hand, relates the total plastic strains to the current state of stress, and was used in early research of plate buckling problems by Ilyushin [7], Stowell [8] and Bijlaard [9]. When applied to plate instability problems, the flow and deformation theories are at odds with each other, since the deformation theory produces results that agree well with test data, while the flow theory produces buckling loads that are higher than the experimental results. Onat and Drucker [10,11] and Neal [12] attributed the discrepancy in the flow theory to its high sensitivity to initial imperfections, while Sewell [13] suggested that initial buckling solutions using the flow theory were also sensitive to the local yield surface. Material constants such as the shear and strain hardening moduli, as well as the slenderness ratio of the plate, were also found to play a significant role in the difference between the predictions of the bifurcation loads based on the flow theory and on the deformation theory.

Shirvastava [14] studied the inelastic buckling of plates which included shear effects. His results showed that the buckling stresses obtained by the flow and

deformation theories are similar at large plate slendernesses, but the flow theory predictions are much higher than the deformation theory predictions at small plate slendernesses. The inclusion of shear effects was found to lower the buckling loads calculated based on the flow theory, but not to the extent of those calculated from the deformation theory. The finite element method has been used in a number of studies of the inelastic local buckling of plates using the deformation theory [15,16,17]. The finite strip method, on the other hand, was used by Dawe and Kulak [18] and Bradford [19,20] using the flow theory and the expression of Lay [21] for the effective shear modulus, and the solutions compared quite favourably with experimental results for I-section members with residual stresses. Further work using efficient finite strip modelling was reported by Bradford and Azhari [22,23,24], with the latter studies using infinitesimal constitutive relationships that originate from both flow and deformation theories.

Limited studies have been conducted using the Rayleigh-Ritz non-discretisation method to solve the inelastic local plate buckling problem. Uenoya and Redwood [25] combined a conventional Rayleigh-Ritz method with the finite element method in their elasto-plastic bifurcation analysis of perforated plates under various conditions of loading, with the finite element method being used for the bifurcation analysis and the Rayleigh-Ritz method being used for determining the in-plane stresses. It was found that the efficiency of the scheme was dependent on the choice of a suitable deflection function to satisfy the boundary conditions. A similar solution technique was also reported by Kawai and Ohtsubo [26].

Hitherto, no work appears to have been undertaken using the pb-2 formulation of the Rayleigh-Ritz method to study inelastic local buckling. This paper presents such a solution technique, using the flow theory [14] and assuming the validity of Shanley's concept of continuous loading [27]. The method can handle plates of finite length subjected to combined in-plane axial, bending and shear actions, and the efficacy and accuracy of the method are demonstrated. Finally, some illustrative studies are conducted using the pb-2 Rayleigh-Ritz method.

2. Theory

2.1 General

Figure 1 shows a flat rectangular plate in a Cartesian coordinate system that is subjected to in-plane axial, bending and shear actions, and whose edges may be simply supported (S), clamped (C) or free (F). The application of the pb-2 Rayleigh-Ritz technique to the inelastic stability of the plate requires the following solution procedure.

- Definition of a suitable infinitesimal displacement function that satisfies the plate kinematic and geometric boundary conditions.
- Selection of an appropriate theory to describe the elasto-plastic behaviour, together with a suitable yield criterion.
- Analytical application of the Rayleigh-Ritz minimisation procedure.
- Numerical solution of the nonlinear eigenproblem.

These steps are set out in the following. Residual stresses are not included in the formulation, but extending the method to handle residual stresses is not difficult.

2.2 Displacement function

The displacement function used to describe the infinitesimal out-of-plane deformations is a two-dimensional Ritz polynomial function, which uses a two-dimensional simple domain polynomial to model the buckled shape and an additional boundary polynomial for modelling the geometric and kinematic conditions. The out-of-plane buckling deformations w are given by

$$w(\xi, \eta) = \varphi_b(\xi, \eta) \sum_{q=0}^p \sum_{r=0}^q a_m \xi^r \eta^{q-r} \quad (1)$$

where

$$m = \frac{1}{2}(q+1)(q+2) - r \quad (2)$$

and where p is a predefined order of the polynomial such that the freedoms in Eqn. 1 are $\text{DOF} = (p + 1)(p + 2)/2$, φ_b is a boundary polynomial describing the boundary conditions that are a function of the plate geometry and kinematics given in Appendix 1, $\xi = x/a$ and $\eta = y/b$. Equation 1 may be written compactly in tensor form as

$$w = M_{ij} a_i a_j \quad (3)$$

where M_{ij} is an interpolation matrix, and the summation extends from 1 to DOF.

2.3 Total change in potential

The change in total potential of the plate Π is the sum of the increase in the strain energy caused by the infinitesimal plate flexure and the increase in the potential of the applied loads. This follows the well-known theory of Timoshenko and Gere [28], and is given by

$$\begin{aligned} \Pi = & \frac{1}{2} \int_A \left(D_x w_{,xx}^2 + D_y w_{,yy}^2 + 2D_1 w_{,xx} w_{,yy} + 4D_{xy} w_{,xy}^2 \right) dA \\ & - \int_A \left\{ \frac{N_a}{2} w_{,x}^2 + \frac{N_o}{2} (1 - \alpha\eta) w_{,x}^2 + N_s w_{,x} w_{,y} \right\} dA \end{aligned} \quad (4)$$

where N_a , N_o and N_s are the actions per unit length shown in Figure 1, A is the domain under consideration (the area of the plate), and D_x , D_y , D_1 and D_{xy} are orthotropic plate rigidities appropriate for elasto-plastic buckling which are described subsequently.

By substituting Eqn. 3 into Eqn. 4

$$\Pi = \frac{1}{2} k_{ij} a_i a_j \quad (5)$$

where k_{ij} is the flexural stiffness matrix given in Appendix 2, and which depends on the load factor λ defined in a ‘generalised’ sense for either proportional or non-proportional loading.

2.4 Variational solution

In Eqn. 5, the condition $\delta\Pi = 0$ defines the equilibrium, while the condition $\delta^2\Pi = 0$ is the familiar bifurcation or local buckling condition. Since k_{ij} are independent of the Ritz coefficients a_m , the buckling condition is

$$\delta^2\Pi = k_{ij}a_i\delta a_j^2 = 0 \quad (6)$$

and further since the variations δa_j are arbitrary, Eqn. 6 produces the usual buckling eigenproblem

$$k_{ij}a_j = 0 \quad (7)$$

which is of order DOF. For elastic buckling, $k_{ij}(\lambda) = \lambda k_{ij}^*$ where k_{ij}^* are constants, and standard eigenvalue routines enable the buckling load factor λ to be extracted. However, for inelastic buckling, the matrix k_{ij} depends nonlinearly on λ , since the orthotropic plate rigidities D_x , D_y , D_1 and D_{xy} , as well as the applied stresses, depend on λ .

The generalised nature of the load factor is made more specific, without loss of generality, by defining the non-proportional loading regime of this paper in which an axial multiplier α_b is applied to the initial curvature shown in Figure 1, while the axial and shear actions shown in this figure remain constant. Assuming an initial value of α_b , the entries $k_{ij}(\alpha_b)$ are assembled, and the matrix $[k]$ is reduced to upper triangular form using Gaussian elimination without row interchanges. The number of eigenvalues of $[k]$ which are less than the trial loading level α_b is equal to the number of negative diagonal elements in the reduced $[k]$ matrix, so for the fundamental mode the loading level for which one negative diagonal exists is sought. The second condition of the eigenproblem is that the determinant of the reduced $[k]$ matrix should equal unity. Hence, once load levels that produce eigenvalues of this matrix less than and greater than unity have been identified, the method of bisections is invoked to converge upon the critical value of α_b . In this manner, accidental convergence on higher modes can be eliminated, and the bisections method, although only a first order iterative scheme,

alleviates convergence difficulties that usually arise with higher order schemes owing to the poorly-behaved eigenvalue function.

2.5 Modelling inelasticity

The method used in this paper is a simplification of the material behaviour appropriate to infinitesimal buckling displacements, which uses a von Mises yield surface but which does not allow for unloading from this surface. The analysis is thus pseudo-elastic, in that regions of the plate subjected to an axial stress σ_x (produced by the bending and axial actions) and shear stress τ for which the effective stress applicable to the loading in Figure 1, given by

$$\sigma_e = \sqrt{\sigma_x^2 + 3\tau^2} \quad (8)$$

satisfies

$$\sigma_e < f_y; \quad (9)$$

the region is entirely elastic, and identified as a region $E \in A$, where f_y is the uniaxial yield stress. On the other hand, whenever $\sigma_e \geq f_y$, an entirely inelastic region of the plate $P \in A$ of the plate is identified, so that the plate area $A = E \cup P$ and $E \cap P = \emptyset$.

For the non-proportional loading regime used in the present study, it is easier to consider the strains rather than stresses, for which the effective strain for plane stress analysis with only end and shear loading (producing $\sigma_y = 0$) given by

$$\varepsilon_e = \sqrt{\varepsilon_x^2 + \frac{\gamma_{xy}^2}{3}} \quad (10)$$

is used. By defining the axial strain multiplier α_b and the shear strain multiplier α_s by

$$\varepsilon_x = \alpha_b \varepsilon_{yield} \quad \gamma_{xy} = \alpha_s \gamma_{yield} \quad (11)$$

where $\varepsilon_{yield} = f_y / E$ and $\gamma_{yield} = \sqrt{3} \left(f_y / E \right)$ (which uses $E/2(1+\nu_p) = E/3$ as the shear modulus at yield, where the plastic Poisson's ratio $\nu_p = 1/2$), then Eqns. 10 and 11 produce

$$\frac{\varepsilon_e}{\varepsilon_{yield}} = \sqrt{\alpha_b^2 + \alpha_s^2} \quad (12)$$

In the non-proportional loading scheme, α_s is set as less than unity, and the value of α_b that defines the start of the inelastic region P is

$$\alpha_b = \sqrt{1 - \alpha_s^2} \quad (13)$$

The iterations on the bending curvature used in the solution of Eqn. 7 thus define uniquely the elastic region E and the inelastic region P of the domain A . Ignoring residual stresses, the axial stress σ_x can be calculated from the axial strain ε_x using

$$\sigma_x = \int_0^{\varepsilon_x} E_t d\varepsilon_x \quad (14)$$

where E_t is the tangent modulus. For the elastic-plastic-strain hardened constitutive relationship used herein and shown in Figure 2, $E_t = E$ in the elastic region E , and either 0 or E_{st} in the inelastic region P .

Nonlinearity arises not only in the actions per unit length in the second integrand of Eqn. 4, but also in the first integrand as the constitutive properties are not constant, and depend on the loading. In the elastic region $E(\alpha_b)$ of the plate, the orthotropic plate rigidities are simply their isotropic elastic values given by

$$D_x = D_y = \frac{Et^3}{12(1-\nu^2)}, \quad D_l = \nu D_x \quad D_{xy} = \frac{Et^3}{24(1+\nu)} \quad (15)$$

where t is the plate thickness and ν is the elastic Poisson's ratio. Consistent with the bifurcative nature of the buckling deformations w and of Shanley's concept of continuous loading, and with the assumption of a thin plate which yields simultaneously through its thickness, strain reversal does not occur and so the incremental statement of the plasticity law [5] may be stated in terms of orthotropic plate rigidities that are based on simple continuous loading defined by the path parameter α_b . Hence in the inelastic region $P(\alpha_b)$ of the plate [22]

$$D_x = \frac{Et^3}{12} \frac{\psi + 3 + 3e}{\psi(5 + 4\nu + 3e) - (1 - 2\nu)^2} \quad (16)$$

$$D_y = \frac{Et^3}{3} \frac{\psi}{\psi(5 - 4\nu + 3e) - (1 - 2\nu)^2} \quad (17)$$

$$D_z = \frac{Et^3}{6} \frac{\psi - 1 + 2\nu}{\psi(5 - 4\nu + 3e) - (1 - 2\nu)^2} \quad (18)$$

$$D_{xy} = \frac{Et^3}{12} \frac{1}{2 + 2\nu + 3e} \quad (19)$$

where

$$\psi = \frac{E}{E_t} \quad (20)$$

$$e = \frac{E}{E_s} - 1 \quad (21)$$

where E_t and E_s are the tangent and secant moduli respectively. In this study, the flow theory is used for which $e = 0$. Other models of plasticity suitable for plate bifurcation are given in Ref. 22.

Finally, the region P consists of a subdomains $P^{pl}(\alpha_b)$ and $P^{st}(\alpha_b)$ that are perfectly plastic (with $E_t = 0$) or strain hardened (with $E_t = E_{st}$) respectively. It is assumed here that uniaxial strain hardening at $\varepsilon_x = \zeta \varepsilon_{yield}$ corresponds to the condition $\varepsilon_e = \zeta \varepsilon_{yield}$ in Eqn. 12. Hence using Eqn. 13, the subdomains $P^{pl}(\alpha_b)$ and $P^{st}(\alpha_b)$ are defined in the non-proportional loading scheme by

$$\sqrt{1 - \alpha_s^2} \leq \alpha_b < \sqrt{\zeta^2 - \alpha_s^2} \quad (\text{perfectly plastic } P^{pl}) \quad (22)$$

$$\alpha_b > \sqrt{\zeta^2 - \alpha_s^2}, \quad (\text{strain hardened } P^{st}) \quad (23)$$

3. Verification and convergence

3.1 General

The theory was coded in FORTRAN and a verification of the Ritz-based algorithm was undertaken. This study considers a rectangular plates with a variety of edge conditions, subjected to combinations of applied in-plane axial, bending and shear actions. For all subsequent studies, $E = 200$ GPa, $\nu = 0.3$, $\zeta = 11$ and $E_{st} = E/33$ was used.

3.2 Elastic buckling

Elastic buckling solutions for rectangular plates are widely available in the literature. The elastic buckling coefficient for a particular applied action N may be obtained from

$$k = \frac{Nb}{\pi^2 D} \quad (24)$$

where $D = Et^3/12(1 - \nu^2)$ is the flexural rigidity of the plate. Elastic buckling was modelled in the present analysis by setting the uniaxial yield stress f_y to a very high value.

Table 1 compares the Ritz-based method with existing solutions for various plate edge conditions when subjected to applied axial compression. This figure also shows the degree of the polynomial p as DPOL, which was used to obtain the solutions. The comparison of the local buckling coefficient k_a with those of other investigators for

a range of aspect ratios $\gamma = a/b$ is very good. The local buckling coefficients of plates subjected to pure bending ($\alpha = 2$ in Figure 1) are compared in Table 2 with those presented by other investigators, and the degree of the polynomial required to obtain a satisfactorily-converged solution DPOL is again given. The agreement of the current algorithm with the independent results is again seen to be good.

The non-proportional loading scheme was altered slightly so that the shear parameter α_s was monotonically increased, while α_b was set as zero. As the comparisons are for elastic buckling only, this had no ramifications on the formulations of yield and strain hardening represented in Eqns. 13, 22 and 23. The results are shown in Table 3, and except for some discrepancies for the S-S-S-F edge restraints, the agreement of the present method with the independent studies is good. The combination of pure bending and shear was considered, in which the shear parameter α_s was introduced by means of a shear buckling coefficient k_s in Eqn. 34, and the bending parameter α_b was varied monotonically in the non-proportional loading scheme. Table 4 compares the solutions with those of the Column Research Committee of Japan [28] for plate aspect ratios of 0.5 and 1.0. While the agreement in the buckling coefficients is generally good, there is some discrepancy for high shear loading with $\gamma = 0.5$.

3.3 Convergence

Convergence of the Ritz-based scheme is important in terms of the order of the polynomial DPOL, since the solution of the eigenproblem Eq. 7 that was described in this paper loses efficiency for higher-order polynomials, as $\text{DOF} = \mathcal{O}(\text{DPOL}^2)$, and numerical problems can also arise. Table 5 shows the convergence characteristics of the loading parameter α_b (with $\alpha_s = 0$) under pure bending ($\alpha = 2$ in Figure 1) for a variety of edge conditions that do not include free edges. The plate slenderness was taken as $b/t = 160$, and the yield stress as $f_y = 250$ MPa. It can be seen that convergence with an increase in DPOL is rapid, but spurious results which can fortunately be identified occur with higher degree polynomials, while in some cases a solution cannot be obtained. The no-solution case, denoted *ns*, arises due to numerical instability within the algorithm, in which accumulated round-off errors associated with the high degree of the polynomial produce a stiffness matrix that is not positive definite. The

results in Table 5 were obtained in double precision arithmetic, and although the convergence characteristics can be improved by recourse to quadruple precision arithmetic, as described by the authors in Ref. 2 for constrained or unilateral buckling, the slightly-improved accuracy is at the expense of excessive computational time that is not commensurate with the small increase in the accuracy. In Table 5, it can be seen that the convergence is better for the S-S-S-S plate, and introducing clamped edges produces poorer convergence, especially at high aspect ratios, owing to numerical instability produced by accumulated round-off error in double precision arithmetic.

The convergence of the loading parameter α_b for plates subjected to pure bending and which have at least one edge free is shown in Table 6. It can be seen that the convergence characteristics are better than those of plates without free edges (Table 5), but that convergence difficulties are encountered for plates with large aspect ratios. Similar convergence behaviour was found for plates with axial compressive and shear actions. The difficulty in convergence with clamped plates can be attributed to the boundary polynomial ϕ_b used in Eqn. 1 and given in Appendix 1. The boundary polynomial requires squared terms to enforce the kinematic conditions of zero deflection and slope, in contrast to the lower order terms for free and simply-supported edges, and numerical instability comes into play for large aspect ratios where it is necessary to deploy a higher-order domain polynomial. Because of the definition of α_b in Eqn. 11, values in Tables 5 and 6 for which $\alpha_b \geq 1$ indicate that the buckling solution is inelastic. It can be seen from these tables that the convergence trends are similar for both elastic and inelastic buckling. Despite the computational difficulties that were experienced, suitable results are possible for most boundary conditions below a plate aspect ratio of about 5, and it is only plates with high proportions of clamped edges that cannot be analysed satisfactorily by the present algorithm at higher aspect ratios higher than about 5.

Tables 7 (S-S-S-S) and 8 (C-F-C-F) show the convergence of the loading parameter α_b for a three aspect ratios with the shear loading parameter α_s set equal to 0.0 or 0.5 in a non-proportional loading scheme. For $\alpha_s = 0$, values of α_b greater than unity are in the inelastic range of structural response, while for $\alpha_s = 0.5$, values of α_b

greater than 0.8660 indicate inelastic buckling. Generally, use of a ninth order polynomial results in convergence up to at least the fourth significant figure, but numerical instabilities preclude most solutions beyond a tenth order polynomial in double precision arithmetic owing to numerical instabilities. Equal numbers of terms were taken for the simple polynomial in the ξ and η directions, irrespective of the symmetry of the loading. Where symmetry does exist, the antisymmetric terms do not contribute to the solution, and *vice versa*. Because of this, the results for $\gamma = 1$ show superior convergence to those at higher aspect ratios, since polynomials of higher order are required for longer plates in order to isolate the multiple buckling eigenmodes. Tables 7 and 8 illustrate, however, that solutions of sufficient accuracy are obtainable for plates with an aspect ratio of at least 3.

Under combined shear and bending, it was found again that the convergence behaviour with increasing polynomial order led to the onset of early numerical instabilities using double precision arithmetic. This numerical instability only occurred for larger plate aspect ratios, which require the use of a polynomial of high degree to isolate the buckling load.

4. Illustration

4.1 General

A short parametric study has been undertaken to illustrate the efficacy of the Ritz-based algorithm. This study generated interaction curves for bending and compression, bending and shear and compression and shear. The modified plate slenderness λ_e in these studies was written in the form [36]

$$\lambda_e = \frac{b}{t} \sqrt{\frac{f_y}{250}} \quad (25)$$

where the uniaxial yield stress f_y has the units of MPa.

4.2 *Interaction of bending and compression*

The local buckling of a S-S-S-S plate of aspect ratio $\gamma = 1.0$ subjected to varying bending gradient α in Figure 1 has been studied. The study used a domain polynomial with DPOL = 9. Figures 3 and 4 plot the normalised critical strain $\varepsilon_{cr}/\varepsilon_{yield}$ and stress σ_{cr}/f_y respectively as a function of λ_e , and which show the attainment of first yield and buckling in the strain-hardening region. A large plastic plateau can be seen for the case of pure bending ($\alpha = 2$), while this is plateau is virtually negligible for pure compression ($\alpha_b = 0$). The latter observation is consistent with the plate entering the perfectly-plastic state at first yield, for which the stress in Eqn. 14 is constant at f_y throughout the plate and term $\psi \rightarrow \infty$ in Eqn. 20. Figure 4 compares three of the loading conditions with the solutions of Timoshenko and Gere [28], and demonstrates good correlation.

4.3 *Interaction of bending and shear*

A plate with S-S-S-S edges, and one with C-F-C-F edges, and subjected to pure bending and shear has been studied. In this non-proportional loading scheme, the shear loading parameter α_s was set as a constant and the axial parameter α_b was varied in the algorithm to obtain the critical bending stress. Figures 5 and 6 show the normalised critical strain and stress for the S-S-S-S plate, while Figures 7 and 8 show these values for the C-F-C-F plate. In both studies, a polynomial with DPOL = 9 was used, and the plate had an aspect ratio $\gamma = 1.0$. It can be seen that the plate slenderness to at which the section becomes fully plastic decreases as the shear loading increases, as does the length of the plastic plateau.

4.4 *Interaction of compression and shear*

The interaction between pure compression and shear for a S-S-S-S plate with an aspect ratio $\gamma = 1.0$ has been studied. As in the previous study, the shear parameter α_s was set to be constant, in order to generate a family of curves, and the parameter α_b was calculated in the non-proportional iterative scheme until satisfactory convergence was achieved, and the critical axial stress was then obtained. The normalised critical strains and stresses are shown in Figures 9 and 10 respectively. Again, it can be seen that the

presence of increasing shear decreases the elastic buckling response of the plate, and precipitates early inelastic plate buckling.

5. Conclusions

This paper has described a non-discretisation Ritz-based method of analysis for the inelastic local buckling of rectangular mild steel plates under axial, bending and shear actions. The method made use of the pb-2 formulation of the Rayleigh-Ritz method, and inelasticity was modelled using an ‘infinitesimal’ formulation of the flow theory of plasticity consistent with the bifurcative nature of the nonlinearity. The study appears to be the first investigation of inelastic plate buckling using the efficient pb-2 Rayleigh-Ritz method.

The convergence of the scheme was studied, where the sensitivity of the numerical stability was demonstrated in the choice of the order of the domain polynomial. The use of a ninth order domain polynomial, which is satisfactory for most studies, produces an eigenproblem of order 55, while more-traditional finite element topological discretisation into rectangular elements would result in an eigenproblem that is at least an order of magnitude greater than this. Since the eigenproblem must be solved in an incremental and iterative fashion for both the discretisation and non-discretisation methods, as described in the paper, the computational prowess of the Ritz-based scheme is vastly superior to that of the finite element method.

The application of the method, in a non-proportional loading scheme, to investigate the inelastic buckling of plates subjected to combined compression and bending, bending and shear and compression and shear has been demonstrated. The efficacy of the procedure produced rapid results in these parametric studies.

6. Acknowledgements

The work reported in this paper was supported by the Australian Research Council under the ARC Large Grants Scheme. The first author was funded by an Australian Postgraduate Award, and by a Faculty of Engineering Dean’s Scholarship provided by The University of New South Wales.

7. References

1. ST Smith, MA Bradford and DJ Oehlers. ‘Local buckling of side-plated reinforced concrete beams. I: Theoretical study’, *Journal of Structural Engineering*, ASCE, 125(6), 622-634, 1999.
2. ST Smith, MA Bradford and DJ Oehlers. ‘Numerical convergence of simple and orthogonal polynomials for the unilateral plate buckling problem using the Rayleigh-Ritz method’, *International Journal for Numerical Methods in Engineering*, 44, 1685-1707, 1999.
3. KM Liew and CM Wang. ‘pb-2 Rayleigh-Ritz method for general plate analysis’, *Engineering Structures*, 15, 55-60, 1993.
4. KM Liew and CM Wang. ‘Vibration analysis of plates by pb-2 Rayleigh-Ritz method: Mixed boundary conditions, re-entrant corners and internal supports’, *Mechanics of Structures and Machines*, 20, 281-292, 1992.
5. PG Hodge. *Plastic analysis of structures*. McGraw-Hill Book Co., New York, 1959.
6. GH Handelman and W Prager. ‘Plastic buckling of a rectangular plate’, NACA Technical Note 1530, 1948.
7. AA Ilyushin. ‘The elasto-plastic stability of plates’, NACA Technical Memorandum 1188, 1947.
8. EZ Stowell. ‘A unified theory of plastic buckling of columns and plates’, NACA Technical Note 1556, 1948.
9. PP Bijlaard. ‘Theory and tests on the plastic stability of plates and shells’, *Journal of the Aeronautical Sciences*, 16, 291-303, 1949.
10. ET Onat and DC Drucker. ‘Inelastic instability and incremental theories of plasticity’, *Journal of the Aeronautical Sciences*, 20, 181-186, 1953.
11. DC Drucker and ET Onat. ‘On the concept of stability of inelastic systems’, *Journal of the Aeronautical Sciences*, 21, 543-548, 1954.
12. KW Neal. ‘Effect of imperfection on the plastic buckling of rectangular plates’, *Journal of Applied Mechanics*, ASME, 42, 115-120, 1975.
13. MJ Sewell. ‘A general theory of elastic and inelastic plate failure II’, *Journal of Mechanics and Physics of Solids*, 12(11), 279-297, 1964.
14. SC Shirvastava. ‘Inelastic buckling of plates including shear effects’, *International Journal of Solids and Structures*, 15, 567-575, 1979.

15. Y Yamada, N Yoshimura and T Sakurai. ‘Plastic stress-strain matrix and its application for the solution of elastic-plastic problems by the finite element method’, *International Journal of Mechanical Sciences*, 10, 343-354, 1968.
16. A Pifko and G Isakson. ‘A finite element method for the plastic buckling of plates’, *AIAA Journal*, 7(10), 1950-1957, 1969.
17. HA El-Ghazaly, RN Dubey and AN Sherbourne. ‘Elasto-plastic buckling of stiffener plates in beam-to-column flange connections’, *Computers and Structures*, 18(2), 201-213, 1984.
18. JL Dawe and GL Kulak. ‘Plate instability of W-shapes’, *Journal of Structural Engineering*, ASCE, 110(6), 1278-1291, 1984.
19. MA Bradford. ‘Local buckling analysis of composite beams’, *Civil Engineering Transactions*, I.E. Aust, CE28(4), 312-317, 1986.
20. MA Bradford. ‘Inelastic buckling of fabricated I-beams’, *Journal of Constructional Steel Research*, 7, 317-334, 1987.
21. MG Lay. ‘Flange local buckling in wide-flanged shapes’, *Journal of the Structural Division*, ASCE, 91(ST6), 95-116, 1965.
22. M Azhari and MA Bradford. ‘Inelastic local buckling of plates with and without residual stresses’, *Engineering Structures*, 15(1), 31-39, 1993.
23. MA Bradford and M Azhari. ‘Local buckling of I-sections bent about the minor axis’, *Journal of Constructional Steel Research*, 31, 73-89, 1994.
24. MA Bradford and M Azhari. ‘Inelastic local buckling of plates and plate assemblies using bubble functions’, *Engineering Structures*, 17(2), 95-103, 1995.
25. M Uenoya and RG Redwood. ‘Elasto-plastic shear buckling of square plates with circular holes’, *Computers and Structures*, 8, 291-300, 1978.
26. T Kawai and M Ohtsubo. ‘A method of solution for the complicated buckling problems of elastic plates with combined use of the Rayleigh-Ritz’s procedure in the finite element method’, Proceedings of the 2nd Air Force Conf. on Matrix Methods in Structural Mechanics, Wright-Patterson Air Force Base, AFFDL-TR-68-150, 967-994, 1968.
27. FR Shanley. ‘Inelastic column theory’, *Journal of the Aeronautical Sciences*, 14(5), 261-268, 1947.
28. SP Timoshenko and JM Gere. *Theory of elastic stability*. 3rd edn., McGraw-Hill, New York, 1961.

29. K Sezawa and W Watanabe. 'Buckling of a rectangular plate with four clamped edges re-examined with an improved theory', *Report of the Aeronautical Research Institute of Tokyo Imperial University*, Vol. 11, 1936, 407-418.
30. HL Cox. 'The buckling of thin plates in compression', *R&M*, No. 1554, London, 1933.
31. M Pignataro, N. Rizzi and A Luongo. *Stability, bifurcation and postcritical behaviour of elastic structures*, Elsevier, Amsterdam, 1991.
32. Column Research Committee of Japan. *Handbook of structural stability*. Corona Publishing Co., Tokyo, 1971.
33. PS Bulson. *The stability of flat plates*. Chatto & Windus, London, 1970.
34. M Stein and J Neff, 'Buckling stress of simply supported rectangular flat plates in shear', NACA Technical Note No. 1222, 1947.
35. B Budiansky and RW Connor, 'Buckling stresses of clamped rectangular flat plates in shear', NACA Technical Note No. 1559, 1948.
36. NS Trahair and MA Bradford. *The behaviour and design of steel structures to AS4100. 3rd en.*, E&FN Spon, London, 1998.

APPENDIX 1 - BOUNDARY POLYNOMIAL φ_b

Edge boundary conditions	Boundary polynomial $\varphi_b(\xi, \eta)$
S-S-S-S	$\xi^1 \eta^1 (\xi - 1)^1 (\eta - 1)^1$
C-C-C-C	$\xi^2 \eta^2 (\xi - 1)^2 (\eta - 1)^2$
C-S-C-S	$\xi^2 \eta^1 (\xi - 1)^2 (\eta - 1)^1$
C-F-C-F	$\xi^1 \eta^0 (\xi - 1)^1 (\eta - 1)^0$

APPENDIX 2 - FLEXURAL STIFFNESS MATRIX k_{ij}

The stiffness matrix for the plate k_{ij} may be written as

$$k_{ij} = k_{1ij} - k_{2ij}$$

where

$$k_{1ij} = \frac{D_x}{\gamma^2} I_y^{2020} + \gamma^2 D_y I_y^{0202} + D_1 \left\{ I_y^{2002} + I_y^{0220} \right\} + 4D_{xy} I_y^{1111}$$

$$k_{2ij} = 12 \left(\frac{b}{t} \right)^2 \left\{ \sigma_a I_y^{1010} + \sigma_b I_y^{1010} (1 - \eta) + 2\gamma (I_y^{0110} + I_y^{1001}) \right\}$$

in which D_x , D_y , D_1 and D_{xy} are the orthotropic plate rigidities appropriate to the elastic and inelastic regions of the plate of area A , and where

$$I_y^{pqrs} = \int_A \left\{ \frac{\partial^{p+q}}{\partial \xi^p \partial \eta^q} [\varphi_b(\xi, \eta) \phi_i(\xi, \eta)] \frac{\partial^{r+s}}{\partial \xi^r \partial \eta^s} [\varphi_b(\xi, \eta) \phi_j(\xi, \eta)] \right\} dA$$

Table 1 Comparison of buckling coefficients with existing solutions: Pure compression

Boundary Condition	Analysis	Compression buckling coefficient, k_a					
		$\gamma = 0.5$	1.0	1.5	2.0	2.5	3.0
S-S-S-S (DPOL=10)	Current	6.250	4.000	4.340	4.000	4.134	4.000
	Ref. 28	6.25	4.00	4.34	4.00	4.13	4.00
S-C-S-F (DPOL=10)	Current	4.463	1.652	1.291	1.336	1.385	1.291
	Ref. 28	-	1.70	1.34	1.38	-	-
S-S-S-F (DPOL=11)	Current	4.356	1.402	0.858	0.668	0.581	0.533
	Ref. 28	4.40	1.440	-	0.698	0.610	0.564
C-C-C-C (DPOL=7)	Current	19.192	10.074	8.351	7.869	7.578	7.285
	Ref. 29	19.28	10.04	8.32	7.88	-	-
S-C-S-C (DPOL=8)	Current	7.691	7.691	7.116	6.972	7.003	10.306
	Ref. 30	7.69	7.69	-	-	-	-
C-C-C-F (DPOL=9)	Current	12.356	4.580	2.522	1.926	1.764	1.684
	Ref. 31	-	4.5	2.2	1.9	1.6	1.5
C-S-C-F (DPOL=9)	Current	12.356	4.375	2.176	1.408	1.053	0.891
	Ref. 31	-	4.2	2.0	1.3	1.1	0.8

Table 2 Comparison of buckling coefficients with existing solutions: Pure bending

Boundary Condition	Analysis	Bending buckling coefficient, k_b				
		$\gamma = 0.5$	1.0	1.2	1.5	2.0
S-S-S-S (DPOL=10)	Current	25.528	25.528	24.020	24.112	23.884
	Ref. 28	25.6	25.6	-	24.1	-
S-C-S-C (DPOL=9)	Current	39.671	39.672	40.568	39.671	39.730
	Ref. 32	39.7	39.7	40.7	39.7	39.7
S-S-S-C (DPOL=9)	Current	29.87	25.533	24.148	24.240	23.941
	Ref. 32	26.0	26.0	24.6	-	-
S-F-S-S (DPOL=11)	Current	7.070	2.631	2.118	1.680	1.326
	Ref. 33	8.85	2.85	2.24	1.74	1.35

Table 3 Comparison of buckling coefficients with existing solutions: Pure shear

Boundary Condition	Analysis	Shear buckling coefficient, k_s				
		$\gamma = 1.0$	1.5	2.0	2.5	3.0
S-S-S-S (DPOL=10)	Current	9.325	7.070	6.546	6.033	5.840
	Ref. 34	9.35	7.07	6.59	6.06	5.89
C-C-C-C (DPOL=7)	Current	14.64	11.46	10.25	9.84	9.54
	Ref. 35	14.71	11.50	10.59	-	9.62
S-S-S-F (DPOL=11)	Current	4.769	2.401	1.633	1.289	1.104
	Ref. 32	3.83	2.30	1.72	-	1.45
S-S-S-C (DPOL=9)	Current	10.706	8.952	8.085	7.773	7.554
	Ref. 32	10.98	9.31	8.43	-	7.96
S-C-S-C (DPOL=8)	Current	12.566	10.785	10.011	9.651	9.506
	Ref. 32	12.28	11.12	10.21	9.81	9.61
C-S-C-S (DPOL=8)	Current	12.566	7.816	6.710	6.306	5.929
	Ref. 32	-	7.78	6.70	6.40	6.17

Table 4 Comparison of local buckling coefficients with existing solutions:
Bending and shear: S-S-S-S

γ	Analysis	Bending buckling coefficient, k_b					
		$k_s = 0.0$	8.0	16.0	20.0	24.0	26.9
0.5	Current	25.528	23.816	18.373	13.813	6.968	0.00
	Ref. 32	25.64	24.30	19.94	16.13	10.26	0.00

γ	Analysis	Bending buckling coefficient, k_b					
		$k_s = 0.0$	2.0	4.0	6.0	8.0	9.42
1.0	Current	25.528	24.408	21.850	17.931	11.650	0.00
	Ref. 32	25.64	24.58	22.18	18.43	12.37	0.00

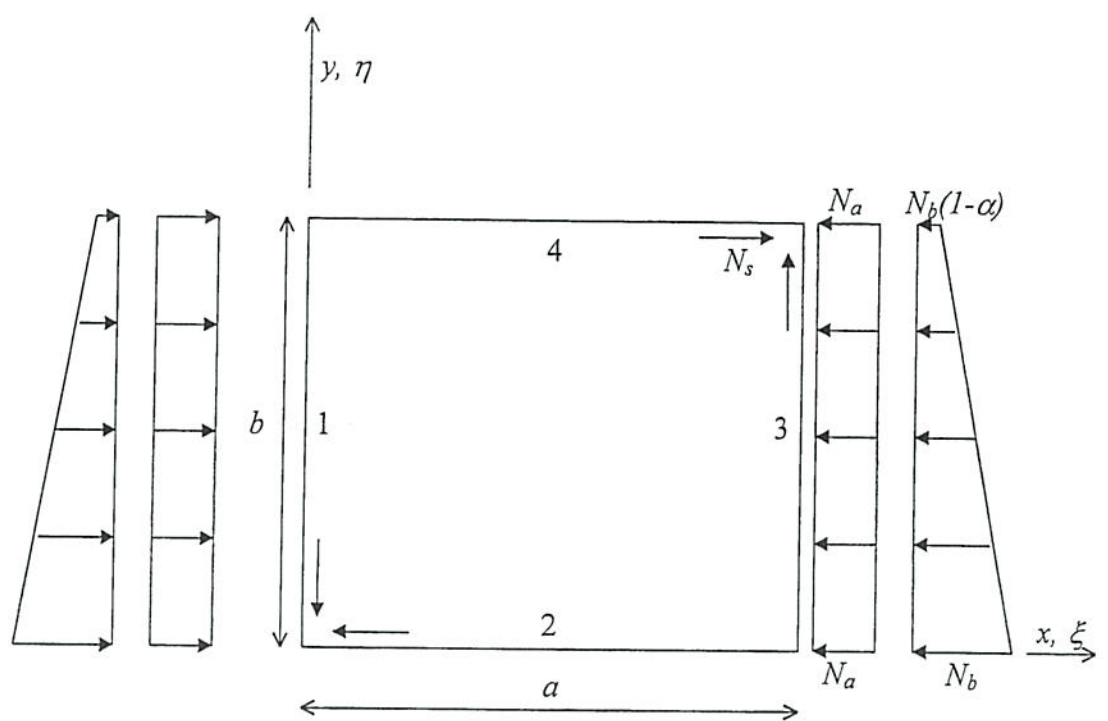


Figure 1 Rectangular Plate

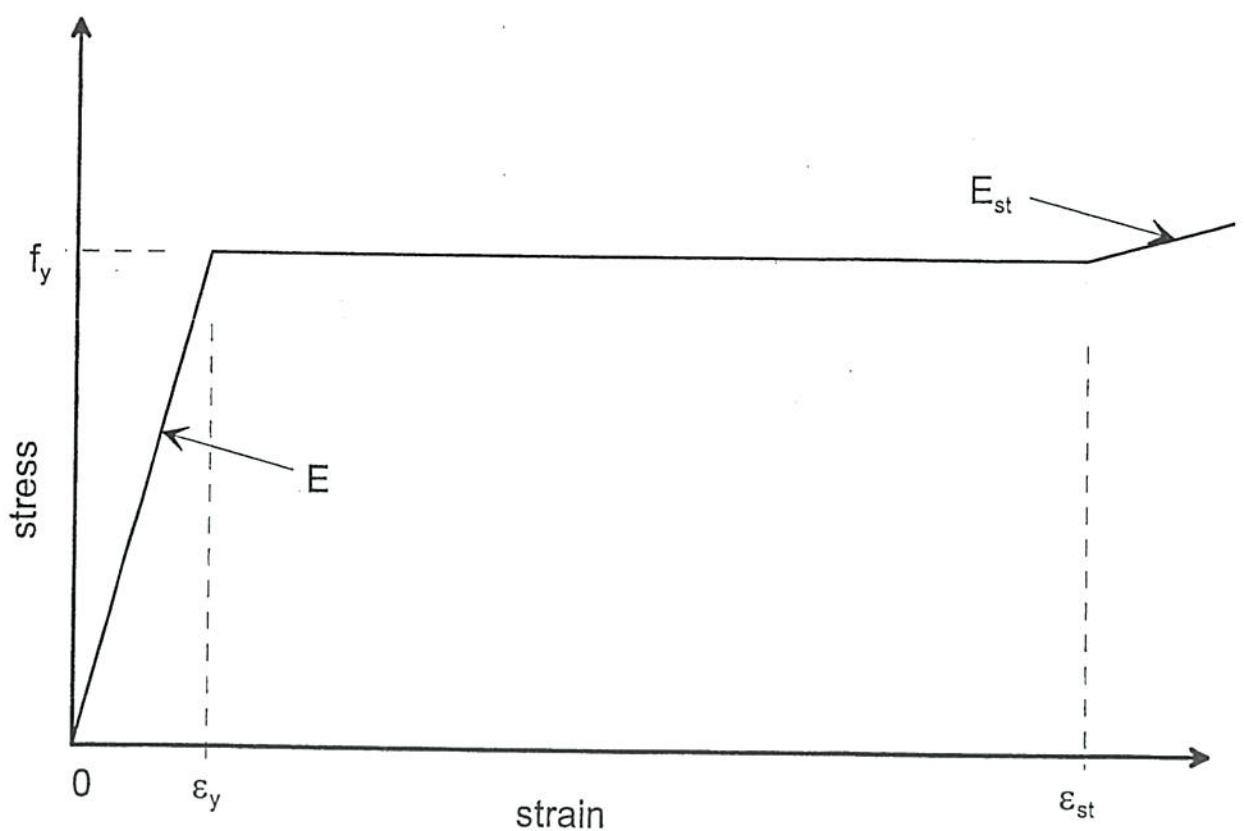


Figure 2 Stress-Strain Relationship

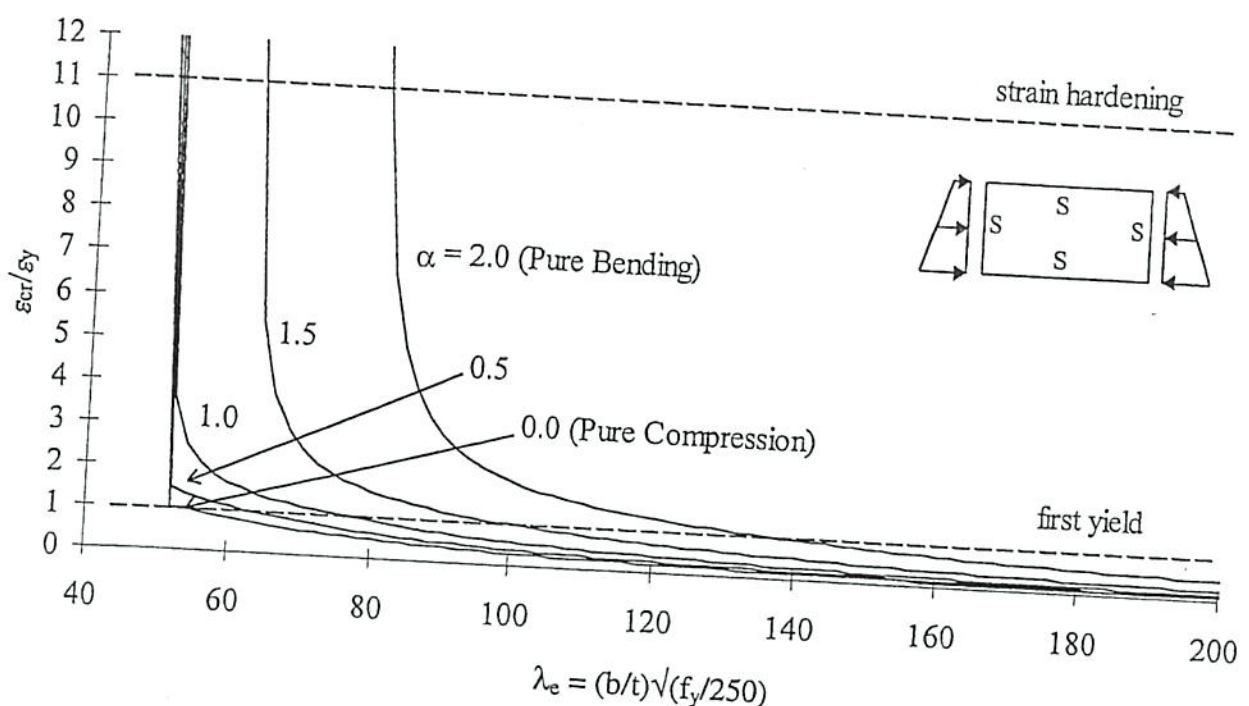


Figure 3 Normalised Critical Strain Under Bending and Compression
(S-S-S-S, $\gamma = 1$)

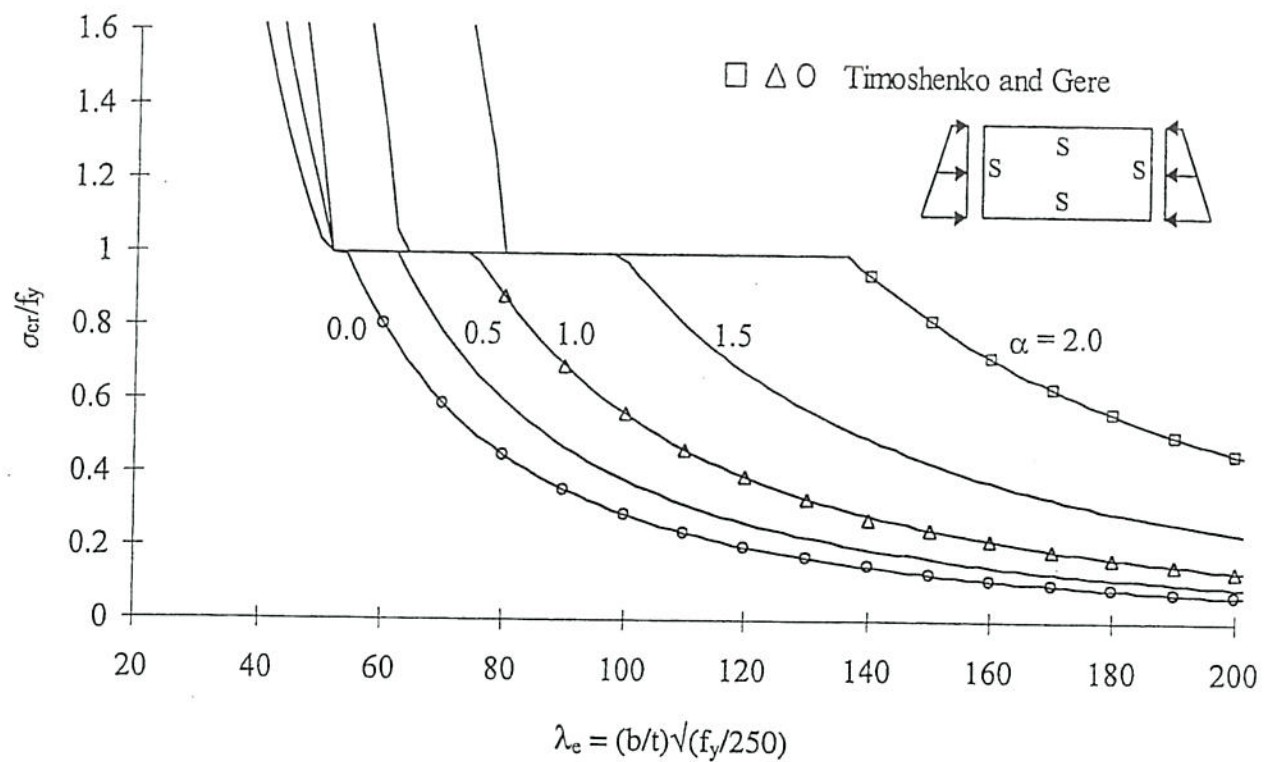


Figure 4 Normalised Critical Stress Under Bending and Compression
(S-S-S-S, $\gamma = 1$)

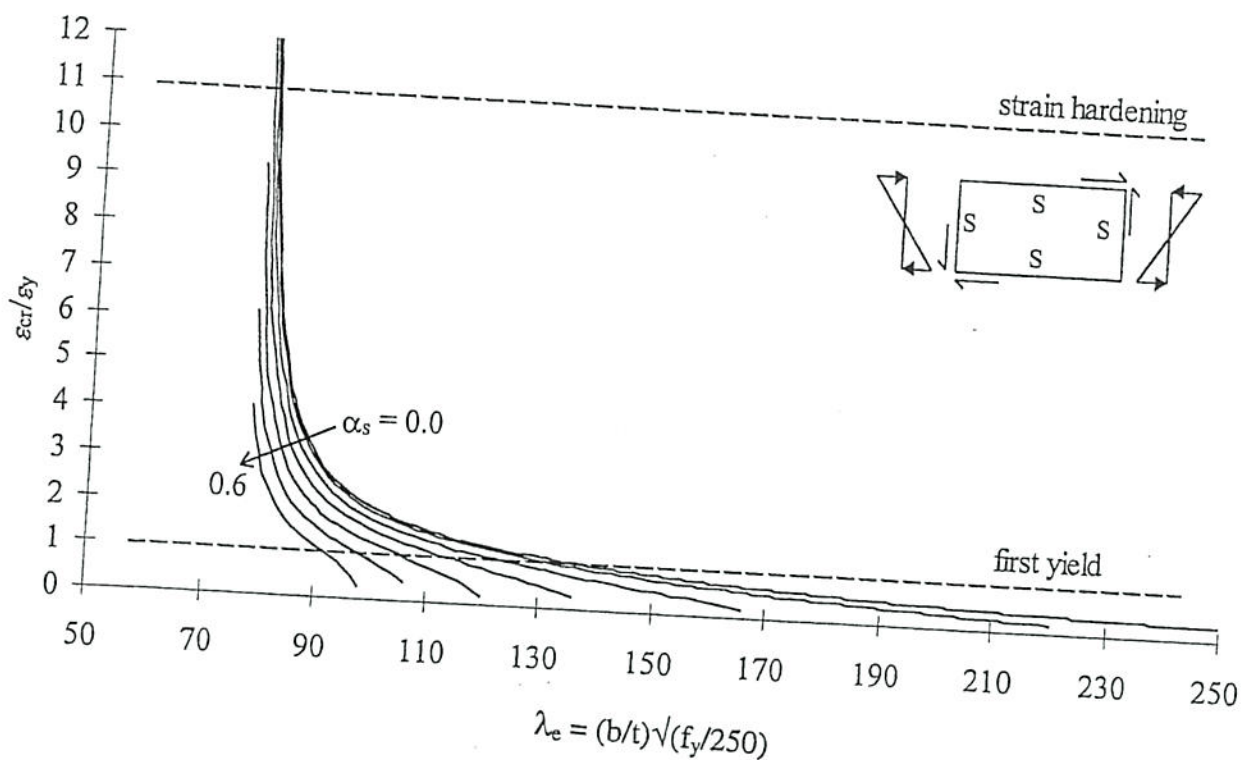


Figure 5 Normalised Critical Strain Under Bending and Shear
(S-S-S-S, $\gamma = 1$)

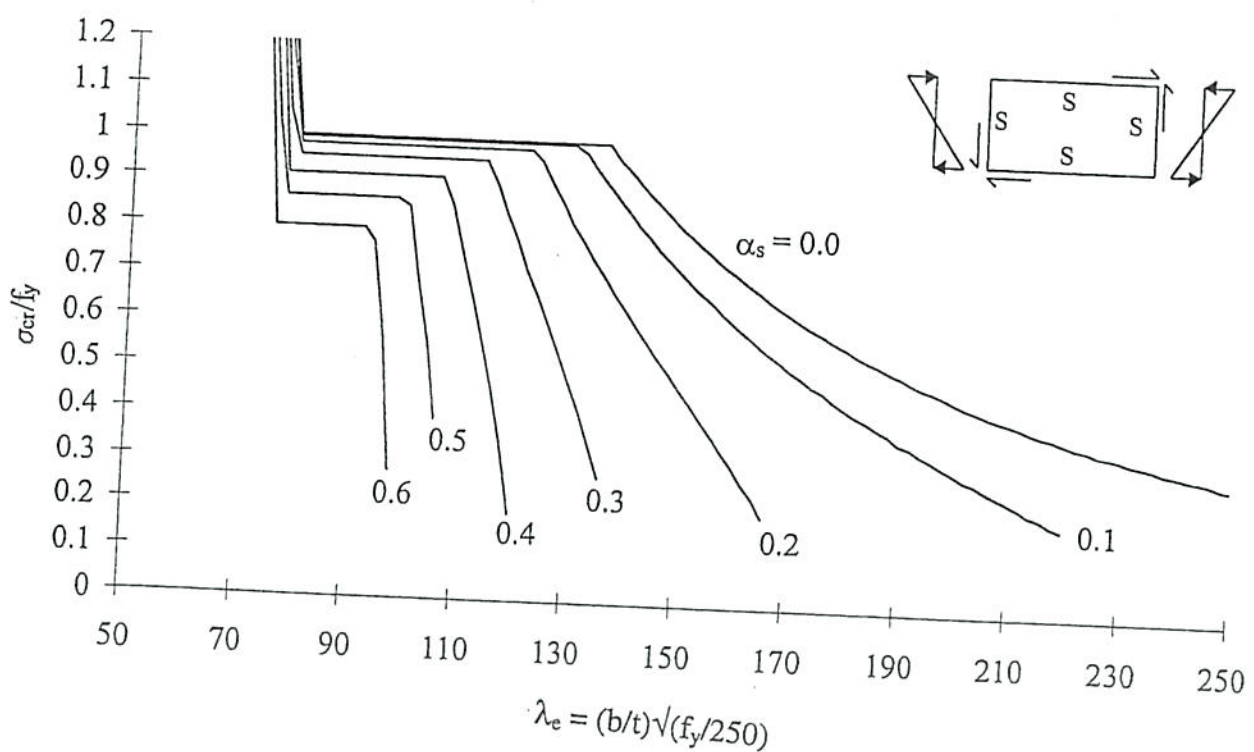


Figure 6 Normalised Critical Stress Under Bending and Shear
(S-S-S-S, $\gamma = 1$)

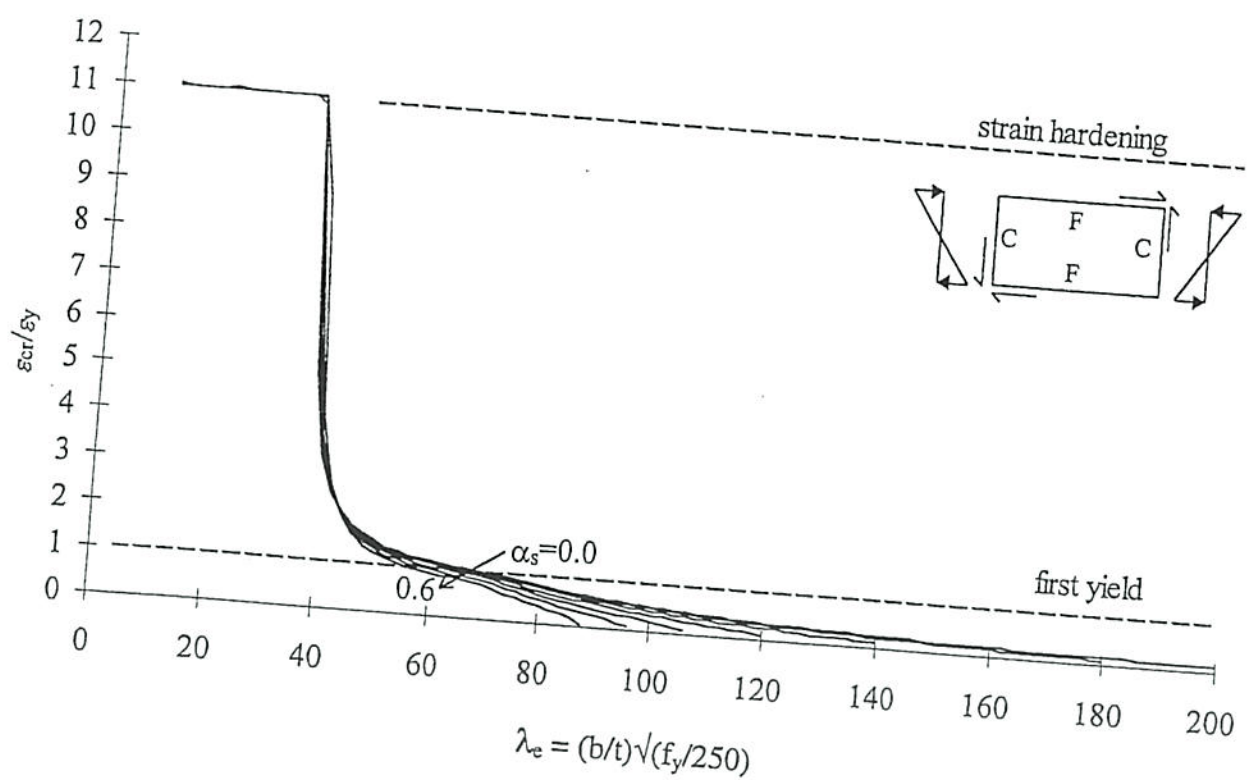


Figure 7 Normalised Critical Strain Under Bending and Shear
(C-F-C-F, $\gamma=1$)

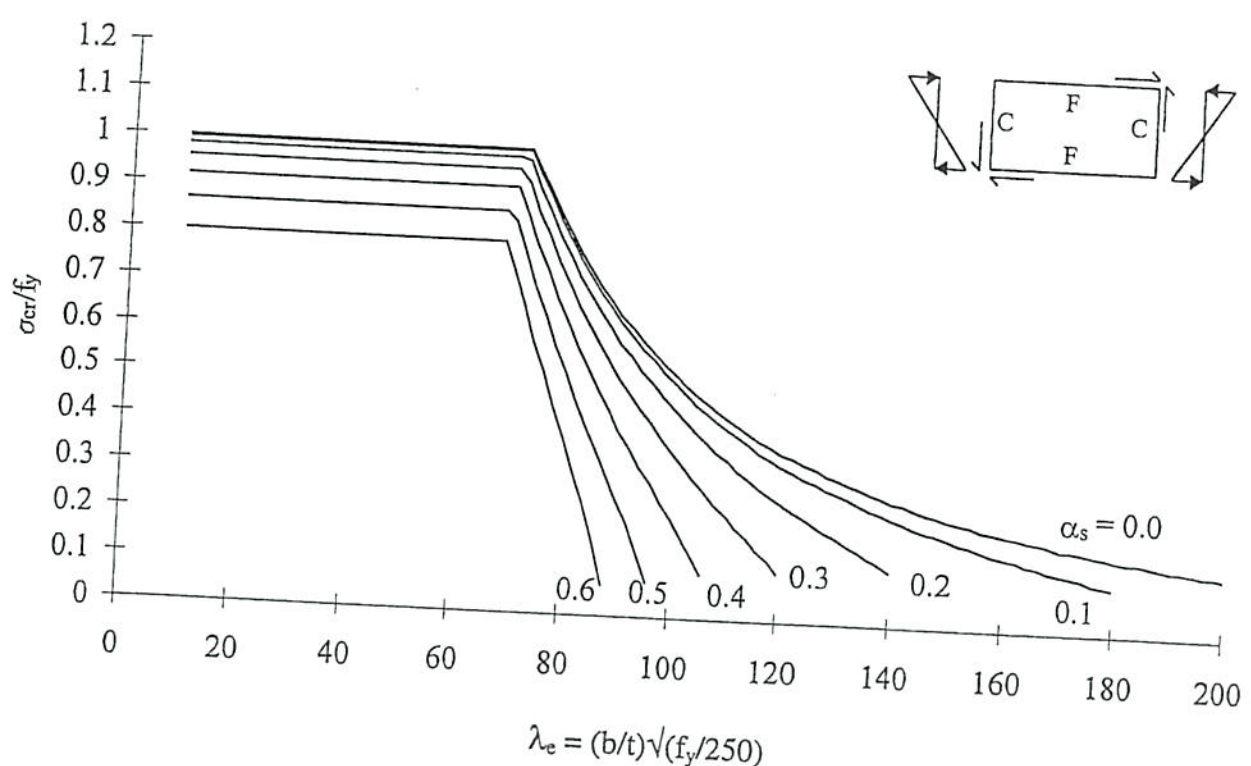


Figure 8 Normalised Critical Stress Under Bending and Shear
(C-F-C-F, $\gamma=1$)

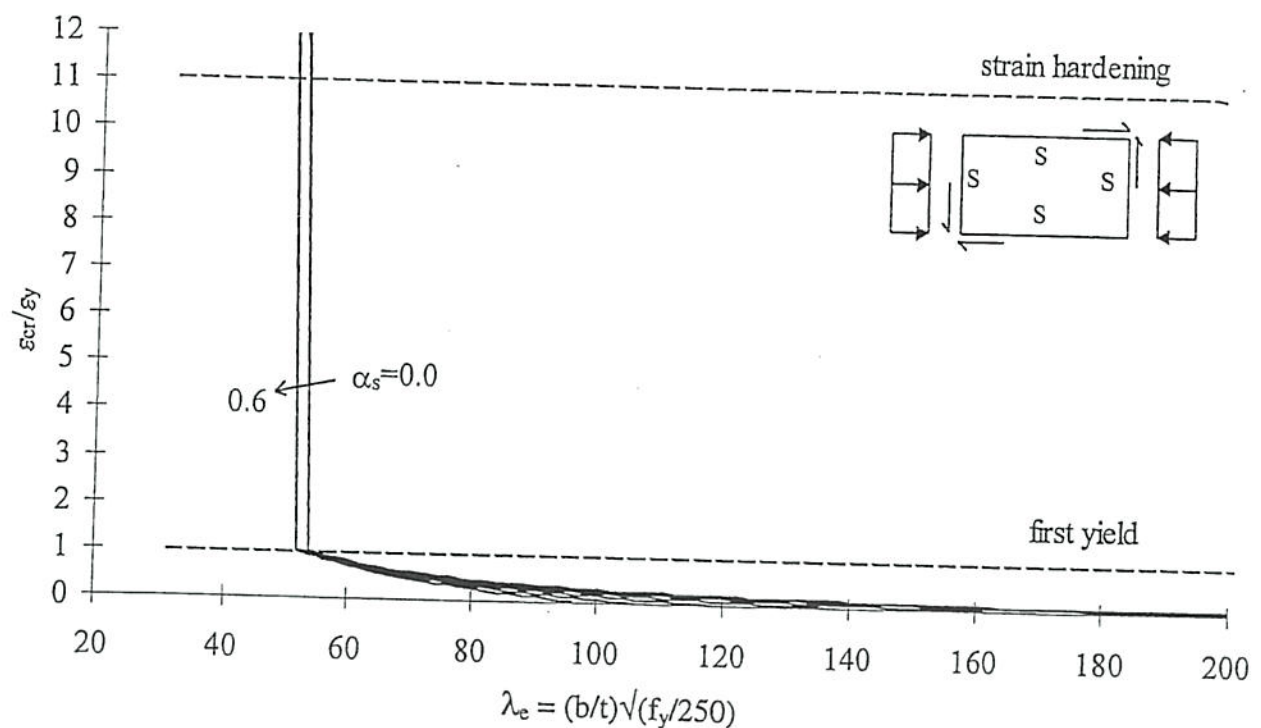


Figure 9 Normalised Critical Strain Under Compression and Shear
(S-S-S-S, $\gamma = 1$)

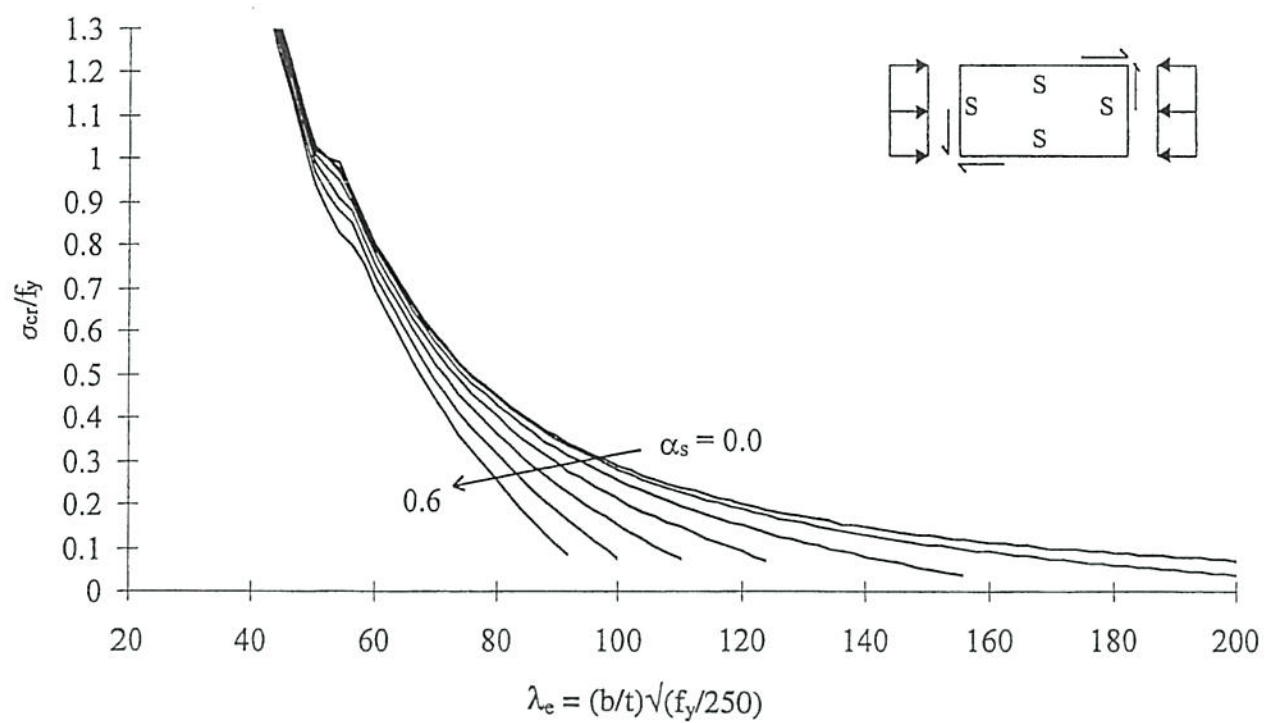


Figure 10 Normalised Critical Stress Under Compression and Shear
(S-S-S-S, $\gamma=1$)